Article

Not peer-reviewed version

fσ8 as a Probe of Future-Singularity Dark Energy Models and ΛCDM

Tomasz Denkiewicz *

Posted Date: 20 November 2025

doi: 10.20944/preprints202511.1604.v1

Keywords: large-scale structure; growth of perturbations; dark energy; dynamical dark energy; cosmological singularities; DESI; Euclid; WFIRST

 doi:10.20944/preprints202511.1604.v1

Article

$f\sigma_8$ as a Probe of Future-Singularity Dark Energy Models and ΛCDM

Tomasz Denkiewicz

Institute of Physics, University of Szczecin, Wielkopolska 15, 70-451 Szczecin, Poland; tomasz.denkiewicz@usz.edu.pl

Abstract

We investigate a class of dark energy models that lead to future cosmological singularities and confront them with observations of the growth of cosmic structure. Using the full linear perturbation formalism, we compute the redshift-space distortion observable $f\sigma_8(z)$ and fit the models to a compilation of growth-rate data. Treating all scenarios on the same footing, we perform parameter estimation and compare the overall quality of the fits obtained for the singularity models and for the concordance ΛCDM cosmology. Our results show which regions of parameter space remain compatible with present growth data and how these models perform relative to ΛCDM, providing a systematic assessment of the viability of future–singularity dark energy scenarios in light of structure formation measurements.

Keywords: large-scale structure; growth of perturbations; dark energy; dynamical dark energy; cosmological singularities; DESI; Euclid; WFIRST

1. Introduction

On cosmological scales, our present knowledge of the late–time expansion is still dominated by purely background, or *geometrical*, measurements. These include the Type Ia supernova Hubble diagram, which constrains the luminosity distance–redshift relation [1–4], the baryon acoustic oscillation scale imprinted in the clustering of galaxies [5–9], and the CMB–based scaled distance indicators to the last–scattering surface, such as $\mathcal{R}$ and l_a [10–12]. Taken together, these probes have firmly established the presence of a dark-energy–like component, allow us to infer its overall abundance, and provide tight constraints on the background expansion history $H(z)$ [13–15]. At the same time, because they are sensitive only to the integrated geometry, they have limited ability to reveal the physical origin of the accelerated expansion. Within general relativity, they do not allow us to clearly distinguish between a cosmological constant (the standard ΛCDM scenario) and a dynamical dark-energy fluid, and in a broader theoretical setting they are not sufficient to decide between GR and modified–gravity explanations.

A complementary avenue is provided by *dynamical* probes, which track the evolution of inhomogeneities through the growth of the matter density contrast, $\delta_m(z) \equiv \delta\rho_m(z)/\rho_m(z)$. Current measurements of the growth rate are still relatively weak, so taken in isolation they do not yet impose very stringent bounds on many cosmological parameters, nor do they strongly discriminate among the broad zoo of dark-energy and modified–gravity models proposed in the literature (see, e.g., [16–20] and references therein). However, when growoh information is combined with the geometrical data, the constraining power increases significantly. In particular, joint analyses of background probes with $\delta_m(z)$–based observables (or derived quantities such as $f\sigma_8$) sharpen our ability to distinguish between dark-energy scenarios and modified–gravity models (including $f(R)$ theories and the Dvali–Gabadadze–Porrati (DGP) model) and the reference ΛCDM cosmology [21–24] far more effectively than either geometrical or dynamical probes considered separately.

The lack of a firm explanation of the origin of the present universe accelerated expansion led to the formulation of different scenarios of modified gravity models or dynamical dark energy models among which, within general relativity, some foresaw different types of singularities in a finite future

 doi:10.20944/preprints202511.1604.v1

time. In this latter field, models describing a Big Rip (BR), a Sudden Future Singularity (SFS), also known as Type II singularities [25–28], a Generalized Sudden Future Singularity (GSFS), a Finite Scale Factor Singularity (FSFS), also known as Type III singularities [28,29], a Big-Separation Singularity (BS) [28] and w-singularities [30] gained some attention among cosmologists.

The new generation of large–scale structure surveys, such as DESI[1] [31], Euclid[2] [32–35] and space missions of the Roman (formerly WFIRST–2.4)[3] type, are designed to deliver high–precision measurements of both background and growth observables. By jointly constraining geometrical quantities (such as distance–redshift relations) and dynamical quantities (encoding the evolution of density perturbations), these experiments are expected to significantly enhance our ability to distinguish a pure cosmological constant from time–varying dark energy scenarios.

In parallel, planned and proposed observations of the cosmic microwave background across microwave to far–infrared frequencies, in both temperature and polarization, will provide complementary information on the dark sector. In particular, mission concepts like PRISM (Polarized Radiation and Imaging Spectroscopy) [36] and the Cosmic Origins Explorer (CoRE) satellite [37], which aim at extremely accurate polarization measurements of the microwave sky, are forecast to tighten constraints on dark energy and possible deviations from ΛCDM [38,39], thereby contributing to a clearer picture of the origin of cosmic acceleration.

DESI has already completed its first year of observations and delivered high–precision measurements of both BAO and the growth rate $f\sigma_8(z)$, which are broadly consistent with the standard ΛCDM scenario and general relativity within current uncertainties, while approaching the regime where scale–dependent growth effects could be detected [40–42]. The Euclid mission has been successfully launched and has entered its main survey phase, with early data releases – including the Early Release Observations (ERO) and the first Quick Data Release (Q1) – demonstrating excellent control of systematics in weak–lensing and large–scale–structure measurements [43–46], although the full tomographic cosmological constraints are still forthcoming. At the same time, some of the CMB polarization concepts mentioned above (PRISM, CoRE) have remained at the level of mission studies rather than operational satellites. These developments confirm the basic premise of our analysis – that forthcoming large–scale–structure surveys are capable of tightly constraining any non–standard, potentially scale–dependent growth – while, at present, showing no compelling observational need to depart from the standard ΛCDM growth history.

In Section 2 we present the background evolution together with the Einstein equations for linear perturbations in the Newtonian gauge. In Section 3 we give a short description of the dynamical dark energy models with the SFS and the FSFS. In Section 4 we describe the compilation of current $f\sigma_8$ measurements and the χ^2 methodology used to confront the models with the data. Finally, in Section 5 we present the results of this comparison.

2. Growth Function

In this section we summarize and adapt the perturbation formalism for the scale-dependent growth function developed in our previous analysis of ΛCDM with future galaxy surveys [47].

The growth of matter inhomogeneities provides a powerful dynamical diagnostic of the expansion history. A convenient quantity is the (logarithmic) growth rate f, defined by

$$f(a) \equiv \frac{d\ln\delta_m(a)}{d\ln a}, \tag{2.1}$$

where δ_m denotes the matter density contrast. In many applications one adopts the phenomenological ansatz

$$f(a) = \Omega_m(a)^\gamma, \tag{2.2}$$

[1] http://desi.lbl.gov/
[2] http://sci.esa.int/euclid/
[3] https://roman.gsfc.nasa.gov/

 doi:10.20944/preprints202511.1604.v1

where a is the scale factor, γ is the so–called growth index, and $\Omega_m(a)$ is the matter density parameter as a function of time,

$$\Omega_m(a) \equiv \frac{H_0^2 \Omega_{m,0} a^{-3}}{H(a)^2}, \tag{2.3}$$

with $\Omega_{m,0}$ the present–day matter density parameter, $H(a) = \dot{a}/a$ the Hubble expansion rate, and H_0 its value today. The parameterization (2.2) provides an approximate solution of the scale–independent growth equation [48,49],

$$f' + f^2 + f\left(\frac{\dot{H}}{H^2} + 2\right) = \frac{3}{2}\,\Omega_m, \tag{2.4}$$

where a prime denotes $' \equiv d/d\ln a$, and which in turn follows from the familiar second–order differential equation for the matter density contrast,

$$\ddot{\delta}_m + 2H\dot{\delta}_m - 4\pi G \rho_m \delta_m = 0, \tag{2.5}$$

after changing the independent variable from cosmic time t to $\ln a$. Here overdots denote time derivatives and ρ_m is the background matter density.

For the standard ΛCDM cosmology one finds $\gamma = 6/11$ [23,50,51], while current data yield an observational estimate $\gamma = 0.665 \pm 0.0669$ [52]. In the case of dark energy models with a slowly varying equation of state, the approximation (2.2) remains accurate, with the growth index given by

$$\gamma = \frac{3(w_0 - 1)}{6w_0 - 5}, \tag{2.6}$$

where $w_0 \equiv w(a) = p/\rho$ denotes the dark energy equation of state (with $w_0 = -1$ for ΛCDM). For such slowly varying dark energy scenarios, γ is expected to be nearly constant in time, with any redshift dependence typically at the level of only a few percent [49,53]. This is no longer true in generic modified gravity models: there the growth index can have a nontrivial time evolution. A well–known example is the Dvali–Gabadadze–Porrati (DGP) model, for which $\gamma \simeq 0.68$, and a more faithful description of the full system (2.10)–(2.12) requires an explicitly redshift–dependent parameterization of $\gamma(z)$. Several such parameterizations have been proposed in the literature [23,24,54–56].

Beyond the scale–independent approximation, it has been shown [48,49,53] that the exact general–relativistic treatment of linear perturbations yields a scale dependence of the growth on sufficiently large scales, already for ΛCDM, with noticeable effects for wavelengths $\gtrsim 100\,h^{-1}$ Mpc. The usual scale–independent treatment assumes that the perturbation modes of interest lie well inside the Hubble radius (sub–Hubble regime). However, this assumption can break down at comparatively modest scales, of order $200\,h^{-1}$ Mpc in the early universe, even though the Hubble radius today is of order $3000\,h^{-1}$ Mpc. The same considerations apply to the ΛCDM model and to the future–singularity dark energy models studied in this work [48,49,53,57].

Furthermore, Denkiewicz [57] showed that dynamical dark energy models with future singularities can exhibit a nontrivial dependence on the perturbation wavenumber: there exists a characteristic scale at which the dark energy perturbations become comparable in amplitude to the matter perturbations. More generally, for any given model one can identify a limiting wavelength below which dark energy perturbations are tightly coupled to matter perturbations and cannot be neglected. While for canonical quintessence fields dark energy inhomogeneities are relevant only on scales comparable to the Hubble radius, models with noncanonical kinetic terms or very small dark energy sound speed, $c_s \ll 1$, can develop dark energy perturbations that trace the matter perturbations even on scales significantly smaller than the Hubble radius [57–60]. The two singular models considered here should be viewed as specific examples within this broader class of possibilities.

In the present analysis we focus on the evolution of dark matter perturbations. We work with the full scale–dependent system of linear perturbation equations for both the FSFS and SFS scenarios, and compare the resulting growth with that obtained in a reference ΛCDM cosmology constructed under the same general assumptions.

 doi:10.20944/preprints202511.1604.v1

We adopt the Newtonian gauge for scalar perturbations and assume negligible anisotropic stress, so that the perturbed line element can be written as

$$ds^2 = -(1+2\Phi)\,dt^2 + (1-2\Phi)\,a^2\gamma_{ij}dx^i dx^j, \tag{2.7}$$

where γ_{ij} denotes the spatial metric and Φ is the Newtonian potential. For a spatially flat universe filled with pressureless, nonrelativistic dark matter with density ρ_m and an exotic dark energy component with density ρ_{de}, the background dynamics is described by the Friedmann and continuity equations,

$$H^2 = \frac{8\pi G}{3}(\rho_m + \rho_{de}), \tag{2.8}$$
$$\dot{\rho} = -3H(\rho + p), \tag{2.9}$$

where $\rho = \rho_m + \rho_{de}$ and p is the total pressure.

Linearizing Einstein's equations around this background in the Newtonian gauge yields, after some algebra, the following evolution equations for the potential Φ, the matter density contrast $\delta \equiv \delta\rho_m/\rho_m$, and the velocity potential of dark matter (encoded in $v_f \equiv -va$):

$$\ddot{\Phi} = -4H\dot{\Phi} + 8\pi G\rho_{de}\,w_{de}\,\Phi, \tag{2.10}$$
$$\dot{\delta} = 3\dot{\Phi} + \frac{k^2}{a^2}v_f, \tag{2.11}$$
$$\dot{v}_f = -\Phi, \tag{2.12}$$

subject to the constraint equations

$$3H(H\Phi + \dot{\Phi}) + \frac{k^2}{a^2}\Phi = -4\pi G\,\delta\rho_m, \tag{2.13}$$
$$(H\Phi + \dot{\Phi}) = -4\pi G\,\rho_m\,v_f. \tag{2.14}$$

Here k denotes the comoving wavenumber of the perturbation mode.

If one assumes that the relevant modes are well inside the Hubble radius, $k^2/a^2 \gg H^2$, and that the gravitational potential varies slowly in time, the system above reduces to the scale–independent evolution equation (2.5) for δ_m. Relaxing only the sub–Hubble assumption, while still keeping the potential quasi–static, leads instead to a scale–dependent growth equation [49,53],

$$\ddot{\delta}_m + 2H\dot{\delta}_m - \frac{4\pi G\rho_m\delta_m}{1+\xi(a,k)} = 0, \tag{2.15}$$

where the function

$$\xi(a,k) = \frac{3a^2H(a)^2}{k^2} \tag{2.16}$$

encodes the departure from the sub–Hubble limit.

Equation (2.15) can be rewritten in terms of the growth rate $f = d\ln\delta_m/d\ln a$ as

$$f' + f^2 + \left(2 - \frac{3}{2}\Omega_m(a)\right)f = \frac{3}{2}\,\frac{\Omega_m(a)}{1+\xi(a,k)}, \tag{2.17}$$

with $' \equiv d/d\ln a$ and, in this expression, assuming the ΛCDM background for $H(a)$. A useful approximate solution of (2.17) is given by

$$f(k,a) = \frac{\Omega_m(a)^\gamma}{1 + \dfrac{3H_0^2\Omega_{m,0}}{ak^2}}, \tag{2.18}$$

 doi:10.20944/preprints202511.1604.v1

which reduces to the standard scale–independent form when $\xi(a,k) \to 0$. In this limit, (2.17) collapses to (2.4), whose solution is well approximated by (2.2) with $\gamma = 6/11$. It has been shown [49,53] that the scale–dependent equation (2.15) reproduces the full general–relativistic system (2.10)–(2.12) with good accuracy up to scales comparable to the horizon; on even larger scales, however, the time evolution of the potential Φ can no longer be neglected.

For the purposes of this work, it is crucial to emphasize that we do not employ either of the approximations mentioned above. In our numerical analysis we solve the complete set of linear perturbation equations without assuming the sub–Hubble limit or a slowly varying gravitational potential.

3. FSFS and SFS as Dynamical Dark Energy Candidates

The SFS and FSFS show up within the framework of the Einstein–Friedmann cosmology governed by the standard field equations, Equations (2.8), and the energy-momentum conservation law, Equation (2.9). We get the SFS and FSFS scenarios with the scale factor in the following form:

$$a(t) = a_s\left[b + (1-b)\left(\frac{t}{t_s}\right)^m - b\left(1 - \frac{t}{t_s}\right)^n\right]. \tag{3.1}$$

An appropriate choice of the constants (b, t_s, a_s, m, n) is necessary [25,61]. For both cases, the SFS as well as the FSFS model, the evolution starts with the standard big-bang singularity at $t = 0$ $(a = 0)$, and evolves to an exotic singularity for $t = t_s$, where $a = a_s \equiv a(t_s)$ is a constant. Accelerated expansion in an SFS universe is assured with a negative b, while for a FSFS universe b has to be positive. In order to have the SFS, n has to be within the range $1 < n < 2$; while for an FSFS, n has to obey the condition $0 < n < 1$. For the SFS at $t = t_s$, $a \to a_s$, $\varrho \to \varrho_s = \text{const.}$, $p \to \infty$; while for an FSFS the energy density ρ also diverges and one has: for $t \to t_s$, $a \to a_s$, $\rho \to \infty$, and $p \to \infty$, where a_s, t_s are constants and $a_s \neq 0$. In both scenarios the non-relativistic matter scales as a^{-3}, i.e.

$$\rho_m = \Omega_{m,0}\rho_0\left(\frac{a_0}{a}\right)^3, \tag{3.2}$$

and the evolution of the exotic (dark energy) fluid ρ_{de}, can be determined by taking the difference between the total energy density ρ, and the energy density of the non-relativistic matter, i.e.

$$\rho_{de} = \rho - \rho_m \ . \tag{3.3}$$

In those scenarios the dark energy component is also responsible for the exotic singularity at $t \to t_s$. The dimensionless energy densities are defined in a standard way as

$$\Omega_m = \frac{\rho_m}{\rho}, \quad \Omega_{de} = \frac{\rho_{de}}{\rho}. \tag{3.4}$$

For the dimensionless exotic dark energy density we have the following expression

$$\Omega_{de} = 1 - \Omega_{m,0}\frac{H_0^2}{H^2(t)}\left(\frac{a_0}{a(t)}\right)^3 = 1 - \Omega_m. \tag{3.5}$$

The barotropic index of the equation of state for the dark energy is defined as

$$w_{de} = p_{de}/\rho_{de}. \tag{3.6}$$

The singularity scenarios considered in this work were also tested as candidates for dynamical fine structure cosmology [62]. In that approach, the dark energy is sourced by a scalar field which couples to the electromagnetic sector of the theory; the knowledge about the effective evolution of the dark energy density and the dark energy equation of state evolution is sufficient to estimate the resulting fine structure evolution.

 doi:10.20944/preprints202511.1604.v1

4. $f\sigma_8$ Data and χ^2 Methodology

In order to confront our models with large-scale-structure measurements, we use the growth observable $f\sigma_8(z)$ and a standard χ^2 methodology.

4.1. Fiducial Cosmological Background

In order to specify the background cosmology for the reference ΛCDM model, we adopt the best-fit Planck 2018 TT,TE,EE+lowE ΛCDM parameters [8] as our fiducial background; the corresponding values are listed in Table 1. In the present analysis these parameters are kept fixed, and Planck data are not included in the $f\sigma_8$ likelihood.

Table 1. Reference ΛCDM parameter set, consistent with the Planck 2018 results, used throughout this work to compute the background expansion and growth of structure for the fiducial ΛCDM model.

$\Omega_c h^2$	$\Omega_b h^2$	Ω_k	h	w	n_s	r	$\ln(A_s 10^{-9})$	τ	z_{re}	$\Omega_\nu h^2$	N_{eff}	Y_{He}	$\sigma_{8,0}$
0.12000	0.02237	0	0.6736	−1	0.9649	0	2.10	0.0544	7.68	0.00065	3.046	0.2454	0.811

The evolution of the matter density contrast is computed by numerically integrating the system of Equations (2.10)–(2.12), subject to the constraint relations (2.13)–(2.14). Throughout this work, the matter contrast δ_m is normalized to unity at $a = 1$.

4.2. Compilation of Current $f\sigma_8$ Measurements

To confront the models with observations we use a compilation of $N = 22$ measurements of the growth observable $f\sigma_8(z)$ obtained from redshift-space distortions (RSD) in galaxy surveys. Our data set coincides with the compilation constructed in Sagredo et al. [19], which is based on the "Gold-2017" sample of 18 independent measurements introduced in Nesseris et al. [20] and supplemented by four additional BOSS and VIPERS points. Our implementation follows closely that of Sagredo et al. [19]: we adopt the same data points, redshifts and covariance prescriptions, including the geometrical rescaling factors; see Sagredo et al. [19], Nesseris et al. [20] and the references therein for further details.

Each entry in the compilation provides the effective redshift z_i, the measured value $[f\sigma_8]_i^{\rm obs}$, the quoted 1σ error σ_i, and the matter density parameter of the fiducial cosmology assumed in that analysis, $\Omega_{m,0}^{\rm fid}$.[4] In addition, the compilation includes non-trivial covariance among the three WiggleZ points and among the four SDSS-IV measurements; we encode these correlations in a 22×22 covariance matrix C_{ij}, with the remaining entries taken to be diagonal, i.e. $C_{ij} = \sigma_i^2 \delta_{ij}$ for all other data points.

4.3. Geometrical Rescaling and χ^2 Definition

Following standard practice, we account for the fact that each RSD measurement was obtained assuming a particular fiducial background when mapping observed angles and redshifts to comoving distances. Denoting by $E_{\rm fid}(z)$ and $D_{A,\rm fid}(z)$ the dimensionless Hubble parameter and angular diameter distance in the fiducial cosmology used for a given measurement, and by $E(z)$ and $D_A(z)$ the corresponding quantities in the model under consideration, the leading geometrical correction enters through the combination (see e.g.[20,63]).

$$R(z;\Omega_{m,0}^{\rm fid}) \equiv \frac{E(z)\, D_A(z)}{E_{\rm fid}(z;\Omega_{m,0}^{\rm fid})\, D_{A,\rm fid}(z;\Omega_{m,0}^{\rm fid})}\,. \tag{4.1}$$

Given the theoretical prediction $f\sigma_8^{\rm th}(z)$ for a model with background $E(z)$ and $D_A(z)$, the quantity to be compared to the published measurement is then

$$[f\sigma_8]_i^{\rm model} = R\big(z_i;\Omega_{m,0}^{\rm fid}(i)\big)\, f\sigma_8^{\rm th}(z_i)\,, \tag{4.2}$$

[4] In practice, the fiducial cosmology for each data point may include additional parameters beyond $\Omega_{m,0}$, but the dominant effect on the RSD observable is captured by the simple geometrical rescaling described below.

 doi:10.20944/preprints202511.1604.v1

where $\Omega_{m,0}^{\rm fid}(i)$ is the fiducial matter density parameter used in the i-th RSD analysis.

We assemble the data–theory residual vector

$$V_i \equiv [f\sigma_8]_i^{\rm obs} - [f\sigma_8]_i^{\rm model}, \qquad i = 1, \ldots, N, \tag{4.3}$$

and define the total χ^2 as

$$\chi^2 = \sum_{i,j=1}^{N} V_i \, (C^{-1})_{ij} \, V_j \,, \tag{4.4}$$

where C_{ij} is the full covariance matrix described above.

In this work we evaluate χ^2 for three fixed cosmological models: (i) a reference ΛCDM background calibrated on the *Planck* 2018 parameters of Table 1, treated here as a fixed model with no additional free parameters; (ii) a sudden future singularity (SFS) model with parameters (m, n, b, y_0) chosen to satisfy geometrical probes; and (iii) a finite scale factor singularity (FSFS) model with an analogous parameter choice. In all cases we solve the full scale-dependent perturbation equations presented in Section 2, and construct $f\sigma_8^{\rm th}(z)$ from the synchronous-gauge matter contrast as described in Section 2. We do *not* perform a full multi-parameter MCMC fit; the present analysis is instead a proof-of-concept comparison of fixed, geometry-motivated models against current growth data. We also report the corresponding p-values and the Akaike and Bayesian information criteria (AIC and BIC) under simple assumptions about the effective number of free parameters in each model.

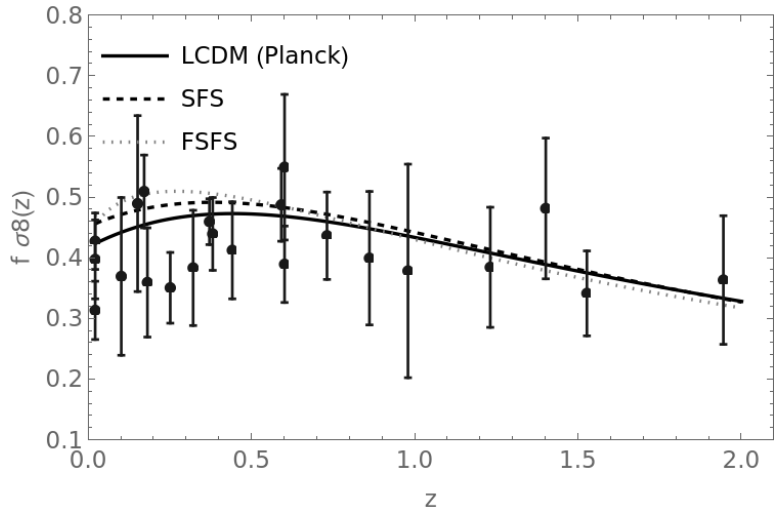

Figure 1. Growth-rate observable $f\sigma_8(z)$ compared with the "Gold" compilation of 22 redshift-space-distortion measurements. Black points with 1σ error bars show the observational data, while the curves denote the theoretical predictions at $k = 0.1\,h\,{\rm Mpc}^{-1}$ for the three fixed backgrounds considered in this work: ΛCDM calibrated to the *Planck* 2018 fiducial cosmology (solid black), the sudden future singularity (SFS) model (black dashed), and the finite scale factor singularity (FSFS) model (grey dotted). For each model we solve the full scale-dependent linear perturbation equations without invoking the sub-Hubble or slowly varying potential approximations, and consistently rescale each data point to the corresponding background geometry via the standard $E(z)D_A(z)$ correction.

5. Results and Conclusions

Using the methodology of Section 4 we first evaluate the growth observable $f\sigma_8(z)$ in the reference ΛCDM model and in the two future-singularity scenarios (SFS and FSFS), for a representative linear scale $k = 0.1\,h\,{\rm Mpc}^{-1}$. For each model we then compute the residual vector V_i and the corresponding χ^2 for the $N = 22$ data points in our $f\sigma_8$ compilation.

For the fixed SFS parameter set used in previous geometrical analyses,[5] we obtain

[5] In the numerical examples shown here we use for SFS: $m = 0.749$, $n = 1.99$, $b = -0.45$, $y_0 = 0.77$ and for FSF: $m = 2/3$, $n = 0.7$, $b = -0.24$, $y_0 = 0.96$; see Dąbrowski et al. [61], Denkiewicz [64], Denkiewicz et al. [65,66], Ghodsi et al. [67] for details and for the constraints from supernovae, BAO, CMB shift parameters and $H(z)$ data.

 doi:10.20944/preprints202511.1604.v1

$$\chi^2_{\rm SFS} \simeq 26.5 \quad \text{for} \quad N = 22\,. \tag{5.1}$$

If we treat this as a pure goodness-of-fit test with $\nu = N$ degrees of freedom, the corresponding p-value is

$$p_{\rm SFS} \simeq 0.23\,, \tag{5.2}$$

so the SFS template provides an acceptable fit to the current $f\sigma_8$ data. The reduced chi-squared is

$$\chi^2_{\nu,\rm SFS} \equiv \frac{\chi^2_{\rm SFS}}{N} \simeq 1.21\,, \tag{5.3}$$

or, if one subtracts an effective number of free parameters $k_{\rm SFS} = 4$ from the data points, $\chi^2_{\nu,\rm SFS} \simeq 1.47$ for $\nu = 22 - 4$.

For the reference ΛCDM model fixed to the Planck 2018 best-fit parameters, solving the full scale-dependent perturbation equations yields

$$\chi^2_{\Lambda\rm CDM} \simeq 17.5\,, \tag{5.4}$$

corresponding to a p-value

$$p_{\Lambda\rm CDM} \simeq 0.74\,, \tag{5.5}$$

i.e. the $f\sigma_8$ data show no tension with this particular growth history. The reduced chi-squared is

$$\chi^2_{\nu,\Lambda\rm CDM} \simeq 0.79 \quad (\nu = 22)\,, \tag{5.6}$$

or $\chi^2_{\nu,\Lambda\rm CDM} \simeq 0.87$ if one subtracts two effective parameters $k_{\Lambda\rm CDM} = 2$ (for $\Omega_{m,0}$ and $\sigma_{8,0}$) and uses $\nu = 22 - 2$.

The difference

$$\Delta\chi^2_{\rm SFS-\Lambda CDM} \equiv \chi^2_{\rm SFS} - \chi^2_{\Lambda\rm CDM} \simeq 9.1 \tag{5.7}$$

quantifies the degradation in the goodness-of-fit when going from the *Planck* ΛCDM background to the SFS model, for the same $N = 22$ data points and without any parameter fitting. While both models yield acceptable absolute p-values, the SFS template is clearly disfavoured in a relative sense.

We have performed an analogous calculation for a representative FSFS parameter set compatible with geometrical probes. In this case the best-fit chi-squared remains larger than in the ΛCDM reference,

$$\chi^2_{\rm FSFS} \simeq 34.3\,, \tag{5.8}$$

which for $N = 22$ data points corresponds to a p-value,

$$p_{\rm FSFS} \simeq 0.05\,. \tag{5.9}$$

The reduced chi-squared is $\chi^2_{\nu,\rm FSFS} \simeq 3.34$ (or $\simeq 4.08$ if we subtract $k_{\rm FSFS} = 4$ from the degrees of freedom), shows that the FSFS benchmark provides noticeably worse fit to the growth data than the *Planck* ΛCDM, but does not reach the level of decisive exclusion. Relative to ΛCDM the degradation in the fit is

$$\Delta\chi^2_{\rm FSFS-\Lambda CDM} \simeq 16.8\,. \tag{5.10}$$

To provide a rough model-comparison diagnostic, we also evaluate the Akaike and Bayesian information criteria,

$$\mathrm{AIC} = \chi^2 + 2k\,, \qquad \mathrm{BIC} = \chi^2 + k\ln N\,, \tag{5.11}$$

where k is the effective number of free parameters entering the $f\sigma_8$ prediction. Taking $k_{\Lambda\rm CDM} = 2$ and $k_{\rm SFS} = k_{\rm FSFS} = 4$, we find for the SFS model

$$\Delta\mathrm{AIC}_{\rm SFS-\Lambda CDM} \simeq 13.1\,, \qquad \Delta\mathrm{BIC}_{\rm SFS-\Lambda CDM} \simeq 15.3\,, \tag{5.12}$$

and for the FSFS model

 doi:10.20944/preprints202511.1604.v1

$$\Delta\mathrm{AIC}_{\mathrm{FSFS}-\Lambda\mathrm{CDM}} \simeq 20\,, \qquad \Delta\mathrm{BIC}_{\mathrm{FSFS}-\Lambda\mathrm{CDM}} \simeq 23\,. \tag{5.13}$$

In both cases the information criteria prefer the standard ΛCDM model over the singularity scenarios; according to common interpretative scales, $\Delta\mathrm{BIC} \gtrsim 10$ already corresponds to "very strong" evidence against the more complex model.

Overall, our analysis shows that:

(i) For the particular fixed parameter sets considered in this work, the SFS and FSFS benchmarks are disfavoured to different degrees with respect to the Planck-2018–calibrated ΛCDM reference model once model complexity is taken into account.

(ii) The FSFS benchmark considered here yelds a poorer fit to the $f\sigma_8$ data than *Planck* ΛCDM and is disfavoured by the information criteria, but it is not decisively ruled out by growth measurements.

We emphasise that these conclusions are based on fixed parameter choices and on a single $f\sigma_8$ compilation, and that we have not performed a joint likelihood analysis including geometrical probes, CMB anisotropies, and the latest full-shape clustering measurements (e.g. DESI DR2). A fully consistent global fit, including a detailed treatment of the DESI and *Euclid* likelihoods and of possible non-linear and biasing systematics, is beyond the scope of this work and is left for future studies. Nevertheless, the present results demonstrate that current growth-of-structure measurements already provide a non-trivial consistency test for future-singularity dark energy models, and that the particular SFS and FSFS templates examined here are not favoured over the standard ΛCDM cosmology.

Author Contributions: Conceptualization, T.D.; methodology, T.D.; formal analysis, T.D.; investigation, T.D.; writing—original draft preparation, T.D.; writing—review and editing, T.D. The author has read and agreed to the published version of the manuscript.

Funding: This research received no external funding.

Institutional Review Board Statement: Not applicable.

Informed Consent Statement: Not applicable.

Data Availability Statement: No new data were created or analyzed in this study. Data sharing is not applicable to this article.

Conflicts of Interest: The author declares no conflict of interest.

Abbreviations

The following abbreviations are used in this manuscript:

ΛCDM	Lambda Cold Dark Matter
SFS	Sudden Future Singularity
FSFS	Finite Scale Factor Singularity
DESI	Dark Energy Spectroscopic Instrument
CMB	Cosmic Microwave Background
BAO	Baryon Acoustic Oscillations
SNeIa	Type Ia Supernovae
LSS	Large-Scale Structure

References

1. Riess, A.G.; et al. Observational Evidence from Supernovae for an Accelerating Universe and a Cosmological Constant. *AJ* **1998**, *116*, 1009–1038, [astro-ph/9805201]. https://doi.org/10.1086/300499.
2. Perlmutter, S.; et al. Measurements of Ω and Λ from 42 High-Redshift Supernovae. *APJ* **1999**, *517*, 565–586, [astro-ph/9812133]. https://doi.org/10.1086/307221.
3. Suzuki, N.; et al. The Hubble Space Telescope Cluster Supernova Survey: V. Improving the Dark Energy Constraints Above z>1 and Building an Early-Type-Hosted Supernova Sample. *Astrophys. J.* **2012**, *746*, 85, [arXiv:astro-ph.CO/1105.3470]. https://doi.org/10.1088/0004-637X/746/1/85.

 doi:10.20944/preprints202511.1604.v1

4. Betoule, M.; et al. Improved Photometric Calibration of the SNLS and the SDSS Supernova Surveys. *Astron. Astrophys.* **2013**, *552*, A124, [arXiv:astro-ph.CO/1212.4864]. https://doi.org/10.1051/0004-6361/201220610.
5. Eisenstein, D.J.; et al. Detection of the Baryon Acoustic Peak in the Large-Scale Correlation Function of SDSS Luminous Red Galaxies. *APJ* **2005**, *633*, 560–574, [astro-ph/0501171]. https://doi.org/10.1086/466512.
6. Bassett, B.A.; Hlozek, R. Baryon Acoustic Oscillations. *arxiv* **2009**, [arXiv:astro-ph.CO/0910.5224].
7. Alam, S.; Ata, M.; Bailey, S.; Beutler, F.; Bizyaev, D.; Blazek, J.A.; Bolton, A.S.; Brownstein, J.R.; Burden, A.; Chuang, C.H.; et al. The clustering of galaxies in the completed SDSS-III Baryon Oscillation Spectroscopic Survey: cosmological analysis of the DR12 galaxy sample. *Monthly Notices of the Royal Astronomical Society* **2017**, *470*, 2617–2652. https://doi.org/10.1093/mnras/stx721.
8. Aghanim, N.; et al. Planck 2018 results. VI. Cosmological parameters. *Astron. Astrophys.* **2020**, *641*, A6, [arXiv:astro-ph.CO/1807.06209]. https://doi.org/10.1051/0004-6361/201833910.
9. Alam, S.; et al. The Completed SDSS-IV extended Baryon Oscillation Spectroscopic Survey: Cosmological Implications from two Decades of Spectroscopic Surveys at the Apache Point observatory **2020**. [arXiv:astro-ph.CO/2007.08991].
10. Bond, J.R.; Efstathiou, G.; Tegmark, M. Forecasting Cosmic Parameter Errors from Microwave Background Anisotropy Experiments. *Mon.Not.Roy.Astron.Soc.291:L33-L41,1997* **1997**, [arXiv:astro-ph/astro-ph/9702100v2]. https://doi.org/10.1093/mnras/291.1.33L.
11. Wang, Y.; Mukherjee, P. Observational Constraints on Dark Energy and Cosmic Curvature. *Phys. Rev.* **2007**, *D76*, 103533, [arXiv:astro-ph/astro-ph/0703780]. https://doi.org/10.1103/PhysRevD.76.103533.
12. Wang, Y.; Dai, M. Exploring uncertainties in dark energy constraints using current observational data with Planck 2015 distance priors. *Phys. Rev.* **2016**, *D94*, 083521, [arXiv:astro-ph.CO/1509.02198]. https://doi.org/10.1103/PhysRevD.94.083521.
13. Weinberg, D.H.; Mortonson, M.J.; Eisenstein, D.J.; Hirata, C.; Riess, A.G.; Rozo, E. Observational Probes of Cosmic Acceleration. *Phys. Rept.* **2013**, *530*, 87–255, [arXiv:astro-ph.CO/1201.2434]. https://doi.org/10.1016/j.physrep.2013.05.001.
14. Salzano, V.; Rodney, S.A.; Sendra, I.; Lazkoz, R.; Riess, A.G.; Postman, M.; Broadhurst, T.; Coe, D. Improving Dark Energy Constraints with High Redshift Type Ia Supernovae from CANDELS and CLASH. *Astron. Astrophys.* **2013**, *557*, A64, [arXiv:astro-ph.CO/1307.0820]. https://doi.org/10.1051/0004-6361/201321738.
15. Lazkoz, R.; Alcaniz, J.; Escamilla-Rivera, C.; Salzano, V.; Sendra, I. BAO cosmography. *JCAP* **2013**, *1312*, 005, [arXiv:astro-ph.CO/1311.6817]. https://doi.org/10.1088/1475-7516/2013/12/005.
16. Ade, P.A.R.; et al. Planck 2015 results. XIII. Cosmological parameters. *arxiv* **2015**, [arXiv:astro-ph.CO/1502.01589].
17. Alam, S.; Ho, S.; Silvestri, A. Testing deviations from LCDM with growth rate measurements from six large-scale structure surveys at z =0.06–1. *Mon. Not. Roy. Astron. Soc.* **2016**, *456*, 3743–3756, [arXiv:astro-ph.CO/1509.05034]. https://doi.org/10.1093/mnras/stv2935.
18. Albarran, I.; Bouhmadi-López, M.; Morais, J. Cosmological perturbations in an effective and genuinely phantom dark energy Universe. *Physics of the Dark Universe* **2017**, *16*, 94–108. https://doi.org/10.1016/j.dark.2017.04.002.
19. Sagredo, B.; Nesseris, S.; Sapone, D. Internal robustness of growth rate data. *Physical Review D* **2018**, *98*, 083543. https://doi.org/10.1103/physrevd.98.083543.
20. Nesseris, S.; Pantazis, G.; Perivolaropoulos, L. Tension and constraints on modified gravity parametrizations of Geff(z) from growth rate and Planck data. *Physical Review D* **2017**, *96*, 023542. https://doi.org/10.1103/physrevd.96.023542.
21. Tsujikawa, S.; Gannouji, R.; Moraes, B.; Polarski, D. The dispersion of growth of matter perturbations in f(R) gravity. *Phys.Rev.D80:084044,2009* **2009**, [arXiv:astro-ph.CO/0908.2669v1]. https://doi.org/10.1103/PhysRevD.80.084044.
22. Gannouji, R.; Moraes, B.; Polarski, D. The growth of matter perturbations in f(R) models. *JCAP 0902:034,2009* **2009**, [arXiv:astro-ph/0809.3374v2]. https://doi.org/10.1088/1475-7516/2009/02/034.
23. Linder, E.V.; Cahn, R.N. Parameterized Beyond-Einstein Growth. *Astropart.Phys.28:481-488,2007* **2007**, [arXiv:astro-ph/astro-ph/0701317v2]. https://doi.org/10.1016/j.astropartphys.2007.09.003.
24. Bamba, K.; Lopez-Revelles, A.; Myrzakulov, R.; Odintsov, S.D.; Sebastiani, L. Cosmic history of viable exponential gravity: Equation of state oscillations and growth index from inflation to dark energy era. *Class. Quant. Grav.* **2013**, *30*, 015008, [arXiv:gr-qc/1207.1009]. https://doi.org/10.1088/0264-9381/30/1/015008.
25. Barrow, J.D. Sudden future singularities. *Class. Quant. Grav.* **2004**, *21*, L79–L82, [arXiv:gr-qc/gr-qc/0403084]. https://doi.org/10.1088/0264-9381/21/11/L03.

26. Barrow, J.D.; Tsagas, C.G. Structure and stability of the Lukash plane-wave spacetime. *Class. Quant. Grav.* **2005**, *22*, 825–840, [arXiv:gr-qc/gr-qc/0411070]. https://doi.org/10.1088/0264-9381/22/5/005.
27. Dabrowski, M.P. Inhomogenized sudden future singularities. *Phys. Rev.* **2005**, *D71*, 103505, [arXiv:gr-qc/gr-qc/0410033]. https://doi.org/10.1103/PhysRevD.71.103505.
28. Nojiri, S.; Odintsov, S.D. Inhomogeneous equation of state of the universe: Phantom era, future singularity and crossing the phantom barrier . *Phys.Rev. D72 (2005) 023003* **2005**, *D72*, 023003, [arXiv:hep-th/hep-th/0505215]. https://doi.org/10.1103/PhysRevD.72.023003.
29. Dąbrowski, M.P.; Denkiewicz, T. Exotic-singularity-driven dark energy, 2009, [arXiv:gr-qc/0910.0023v1].
30. Dąbrowski, M.P.; Denkiewicz, T. Barotropic index w-singularities in cosmology. *Phys. Rev. D 79, 063521 (2009)* **2009**, [arXiv:gr-qc/0902.3107v3]. https://doi.org/10.1103/PhysRevD.79.063521.
31. Levi, M.; et al. The DESI Experiment, a whitepaper for Snowmass 2013. *arxiv* **2013**, [arXiv:astro-ph.CO/1308.0847].
32. Cimatti, A.; Laureijs, R.; Leibundgut, B.; Lilly, S.; Nichol, R.; Refregier, A.; Rosati, P.; Steinmetz, M.; Thatte, N.; Valentijn, E. Euclid Assessment Study Report for the ESA Cosmic Visions. *arxiv* **2009**, [arXiv:astro-ph.CO/0912.0914].
33. Refregier, A.; Amara, A.; Kitching, T.D.; Rassat, A.; Scaramella, R.; Weller, J. Euclid Imaging Consortium Science Book. *arxiv* **2010**, [arXiv:astro-ph.IM/1001.0061].
34. Laureijs, R.; et al. Euclid Definition Study Report. *arxiv* **2011**, [arXiv:astro-ph.CO/1110.3193].
35. Amendola, L.; et al. Cosmology and Fundamental Physics with the Euclid Satellite. *arxiv* **2016**, [arXiv:astro-ph.CO/1606.00180].
36. Collaboration, P.; Andre, P.; et al. PRISM (Polarized Radiation Imaging and Spectroscopy Mission): A White Paper on the Ultimate Polarimetric Spectro-Imaging of the Microwave and Far-Infrared Sky, 2013, [arXiv:astro-ph.CO/1306.2259v1].
37. Collaboration, T.C.; Armitage-Caplan, C.; et al. COrE (Cosmic Origins Explorer) A White Paper, 2011, [arXiv:astro-ph.CO/1102.2181v2].
38. Errard, J.; Feeney, S.M.; Peiris, H.V.; Jaffe, A.H. Robust forecasts on fundamental physics from the foreground-obscured, gravitationally-lensed CMB polarization. *JCAP* **2016**, *1603*, 052, [arXiv:astro-ph.CO/1509.06770]. https://doi.org/10.1088/1475-7516/2016/03/052.
39. Valentino, E.D.; Brinckmann, T.; Gerbino, M.; Poulin, V.; Bouchet, F.; Lesgourgues, J.; Melchiorri, A.; Chluba, J.; Clesse, S.; Delabrouille, J.; et al. Exploring cosmic origins with CORE: Cosmological parameters. *Journal of Cosmology and Astroparticle Physics* **2018**, *2018*, 017–017. https://doi.org/10.1088/1475-7516/2018/04/017.
40. Adame, A.; Others. DESI 2024 VI: Cosmological Constraints from the Measurements of Baryon Acoustic Oscillations. *journal = "JCAP* **2024**. https://doi.org/10.1088/1475-7516/2025/02/021.
41. Adame, A.G.; et al. DESI 2024 V: Full-Shape Galaxy Clustering from Galaxies and Quasars. *JCAP* **2025**, *2025*, 008, [arXiv:astro-ph.CO/2411.12021]. https://doi.org/10.1088/1475-7516/2025/09/008.
42. Adame, A.G.; et al. DESI 2024 VII: Cosmological Constraints from the Full-Shape Modeling of Clustering Measurements. *JCAP* **2025**, *2025*, 028, [arXiv:astro-ph.CO/2411.12022]. https://doi.org/10.1088/1475-7516/2025/07/028.
43. Atek, H.; et al. Euclid: Early Release Observations – A preview of the Euclid era through a galaxy cluster magnifying lens. *Astronomy and Astrophysics* **2025**, *697*, A15. https://doi.org/10.1051/0004-6361/202450776.
44. Aussel, H.; et al. Euclid Quick Data Release (Q1) – Data release overview. *Astron. Astrophys.* **2025**, [arXiv:astro-ph.GA/2503.15302]. in press.
45. Quilley, L.; et al. Euclid Quick Data Release (Q1). Exploring galaxy morphology across cosmic time through S
'ersic fits. *Astron. Astrophys.* **2025**, [arXiv:astro-ph.GA/2503.15309]. in press.
46. Euclid Quick Release Q1. ESA Euclid mission data release, 2025. https://doi.org/10.57780/esa-2853f3b.
47. Denkiewicz, T.; Salzano, V. Testing scale-dependent perturbations in ΛCDM with future galaxy surveys. *Physics of the Dark Universe* **2019**, *25*, 100319. https://doi.org/10.1016/j.dark.2019.100319.
48. Dent, J.B.; Dutta, S. On the dangers of using the growth equation on large scales in the Newtonian gauge, 2009, [arXiv:astro-ph/0808.2689v4]. https://doi.org/10.1103/PhysRevD.79.063516.
49. Dent, J.B.; Dutta, S.; Perivolaropoulos, L. New Parametrization for the Scale Dependent Growth Function in General Relativity. *Phys.Rev.D80:023514,2009* **2009**, [arXiv:astro-ph.CO/0903.5296v2]. https://doi.org/10.1103/PhysRevD.80.023514.
50. Wang, L.; Steinhardt, P.J. Cluster Abundance Constraints on Quintessence Models. *Astrophys.J.508:483-490,1998* **1998**, [arXiv:astro-ph/astro-ph/9804015v1]. https://doi.org/10.1086/306436.

 doi:10.20944/preprints202511.1604.v1

51. Linder, E.V. Cosmic Growth History and Expansion History. *Phys.Rev.D72:043529,2005* **2005**, [arXiv:astro-ph/astro-ph/0507263v2]. https://doi.org/10.1103/PhysRevD.72.043529.
52. Johnson, A.; Blake, C.; Dossett, J.; Koda, J.; Parkinson, D.; Joudaki, S. Searching for Modified Gravity: Scale and Redshift Dependent Constraints from Galaxy Peculiar Velocities. *Mon. Not. Roy. Astron. Soc.* **2016**, *458*, 2725–2744, [arXiv:astro-ph.CO/1504.06885]. https://doi.org/10.1093/mnras/stw447.
53. Perivolaropoulos, L. Consistency of LCDM with Geometric and Dynamical Probes, 2010, [arXiv:astro-ph.CO/1002.3030v1]. https://doi.org/10.1088/1742-6596/222/1/012024.
54. Ishak, M.; Dossett, J. Contiguous redshift parameterizations of the growth index. *Phys.Rev.D80:043004,2009* **2009**, [arXiv:astro-ph.CO/0905.2470v2]. https://doi.org/10.1103/PhysRevD.80.043004.
55. Gannouji, R.; Polarski, D. The growth of matter perturbations in some scalar-tensor DE models. *JCAP 0805:018,2008* **2008**, [arXiv:astro-ph/0802.4196v4]. https://doi.org/10.1088/1475-7516/2008/05/018.
56. Gong, Y. Growth factor parametrization and modified gravity. *Phys.Rev.D78:123010,2008* **2008**, [arXiv:astro-ph/0808.1316v2]. https://doi.org/10.1103/PhysRevD.78.123010.
57. Denkiewicz, T. Dark energy and dark matter perturbations in singular universes. *Journal of Cosmology and Astroparticle Physics* **2015**, *37*, 037, [arXiv:astro-ph.CO/1411.6169v2]. https://doi.org/10.1088/1475-7516/2015/03/037.
58. Abramo, L.R.; Batista, R.C.; Liberato, L.; Rosenfeld, R. Physical approximations for the nonlinear evolution of perturbations in dark energy scenarios. *Phys.Rev.D79:023516,2009* **2008**, [arXiv:astro-ph/0806.3461v1]. https://doi.org/10.1103/PhysRevD.79.023516.
59. Sapone, D.; Kunz, M. Fingerprinting dark energy. *Phys.Rev.D80:083519,2009* **2009**, [arXiv:astro-ph.CO/0909.0007v2]. https://doi.org/10.1103/PhysRevD.80.083519.
60. Batista, R.C.; Pace, F. Structure formation in inhomogeneous Early Dark Energy models. *JCAP 1306 (2013) 044* **2014**, [arXiv:astro-ph.CO/1303.0414v2]. https://doi.org/10.1088/1475-7516/2013/06/044.
61. Dąbrowski, M.P.; Denkiewicz, T.; Hendry, M.A. How far is it to a sudden future singularity of pressure? *Phys.Rev.D75:123524,2007* **2007**, [arXiv:astro-ph/0704.1383v2]. https://doi.org/10.1103/PhysRevD.75.123524.
62. Dąbrowski, M.P.; Denkiewicz, T.; Martins, C.J.A.P.; Vielzeuf, P.E. Variations of the fine-structure constant α in exotic singularity models. *Phys. Rev. D 89, 123512 (2014)* **2014**, [arXiv:astro-ph.CO/1406.1007v1].
63. Beutler, F.; Saito, S.; Seo, H.J.; Brinkmann, J.; Dawson, K.S.; Eisenstein, D.J.; Font-Ribera, A.; Ho, S.; McBride, C.K.; Montesano, F.; et al. The clustering of galaxies in the SDSS-III Baryon Oscillation Spectroscopic Survey: Testing gravity with redshift-space distortions using the power spectrum multipoles. *Mon. Not. R. Astron. Soc.* **2014**, *443*, 1065–1089, [arXiv:astro-ph.CO/1312.4611]. https://doi.org/10.1093/mnras/stu1051.
64. Denkiewicz, T. Observational constraints on finite scale factor singularities, 2012, [arXiv:astro-ph.CO/1112.5447v3]. https://doi.org/10.1088/1475-7516/2012/07/036.
65. Denkiewicz, T.; Dąbrowski, M.P.; Ghodsi, H.; Hendry, M.A. Cosmological tests of sudden future singularities. *Phys.Rev.D85:083527,2012* **2013**, [arXiv:astro-ph.CO/1201.6661v3]. https://doi.org/10.1103/PhysRevD.85.083527.
66. Denkiewicz, T.; Dąbrowski, M.P.; Martins, C.J.A.P.; Vielzeuf, P. Redshift drift test of exotic singularity universes. *Phys. Rev. D 89, 083514 (2014)* **2014**, [arXiv:astro-ph.CO/1402.0520v2]. https://doi.org/10.1103/PhysRevD.89.083514.
67. Ghodsi, H.; Hendry, M.A.; Dąbrowski, M.P.; Denkiewicz, T. Sudden Future Singularity models as an alternative to Dark Energy?, 2011, [arXiv:astro-ph.CO/1101.3984v4]. https://doi.org/10.1111/j.1365-2966.2011.18484.x.